Article

Atmospheric Radon in the Central Mediterranean: Seasonal and Diurnal Variations Measured in Gozo, Malta

Beatriz Defez [1,*], Raymond Ellul [2], Martin Saliba [2], Rebecca Muscat [2], Marvic Grima [2], Alfred Micallef [2], Charles Galdies [3], María Moncho-Santonja [1], Silvia Aparisi-Navarro [1] and Guillermo Peris-Fajarnés [1]

[1] Research Center in Graphic Technologies, Universitat Politècnica de València, 46022 Valencia, Spain; monsan@upv.es (M.M.-S.); silapna@cam.upv.es (S.A.-N.); gperis@upv.es (G.P.-F.)

[2] Department of Geosciences, University of Malta, MSD 2080 Msida, Malta; ray.ellul@um.edu.mt (R.E.); martin.saliba@um.edu.mt (M.S.); rebecca.muscat@um.edu.mt (R.M.); marvic.grima@um.edu.mt (M.G.); alfred.micallef@um.edu.mt (A.M.)

[3] Institute of Earth Systems, University of Malta, MSD 2080 Msida, Malta; charles.galdies@um.edu.mt

[*] Correspondence: bdefez@upv.es; Tel.: +34-96-387-95-18

Abstract: This paper presents the findings of a 12-year study on radon conducted from January 2011 to December 2022 at the Giordan Lighthouse station on the island of Gozo, Malta. Located in the Central Mediterranean, Gozo's strategic position enables effective monitoring of air mass movements between Africa and Europe (from south to north) and between Europe and Central Asia (from west to east). Our research involves an analysis of seasonal and diurnal variations in radon levels, alongside analysis of relevant meteorological variables, clustering of air mass back trajectories, and assessment of local and remote radon production. The findings provide critical insights into the dynamics of atmospheric radon, which are significant not only for the Maltese islands, but also for enhancing our understanding of transcontinental radon transport in the Central Mediterranean, a region that has remained largely unexplored.

Keywords: atmospheric radon; natural radioactivity; Mediterranean Basin

1. Introduction

Atmospheric radon-222 (hereafter referred to as radon) is an inert gas produced through the alpha decay of radium (Ra) in the uranium-238 (U-238) nucleus, with a half-life of 3.82 days. It emanates from various rock and soil types into the atmosphere, as well as into groundwater and surface water [1–4].

Atmospheric radon results from three processes: emanation, migration, and exhalation. Radon emanates from soil and rock particles into pore spaces, migrates as a gas dissolved in groundwater or ground air, and may reach the ground surface through exhalation. Typically, radon is generated from radium decay within mineral grains of soil, necessitating its escape into pore spaces before being transported to the atmosphere via diffusion and convection [5–12].

Radon production is influenced by geographical and environmental factors, including the petrological and mineralogical composition of bedrock, soil permeability and porosity, faulting, shearing, fracturing in bedrock and soil, soil humidity, and atmospheric conditions such as temperature, atmospheric pressure, and wind [13–15].

Nevertheless, the concentration of radon at a specific site is influenced not only by local production, but also by geographical and meteorological factors. The local radon

concentration is a function of radon production, both local and remote, and meteorological variables, whose seasonal dynamics influence radon release and transportation. Air masses can transport radon from both nearby and distant areas, significantly affecting total radon levels. Given radon's half-life of 3.8 days, fetch regions over the previous 14 days may play a role in its measured concentration. Terrestrial radon emissions are typically two to three orders of magnitude greater than those from oceanic sources, leading to a consensus that oceanic contributions to radon concentrations are minimal. As a result, radon external sources are classified as oceanic or terrestrial in the first place. This pronounced land–ocean contrast underscores the importance of non-local or imported radon, particularly in coastal and insular regions [16].

The study of radon is crucial from two perspectives. Firstly, radon contributes significantly to the total dose of natural radioactivity impacting human health, constituting 50% of natural exposure. While outdoor radon levels are typically low and harmless (usually between 5 Bqm^{-3} to 15 Bqm^{-3}), indoor concentrations can escalate in areas with high geocentric radon production and poor ventilation, posing a significant risk for lung cancer. High long-term indoor radon exposure is responsible for 3% to 14% of global lung cancer cases, varying based on national average radon levels and smoking prevalence [17–21].

Secondly, naturally occurring radionuclides like radon are vital isotopes for studying atmospheric processes. Continuous monitoring of radon is encouraged and deemed an essential component of WMO/GAW (World Meteorological Organization/Global Atmospheric Watch) air quality observations. Together with other radionuclide measurements, radon data provide valuable insights for evaluating air transport models and discerning global atmospheric conditions. Radon serves as an excellent tracer for studying vertical mixing and transport of greenhouse gasses, offering a convenient means of estimating air mass contact with terrestrial pollutant sources, atmospheric mixing, and dilution [22–28].

The Mediterranean Basin, renowned for its rich biodiversity and unique climatic conditions, faces unprecedented environmental challenges due to climate change and air pollution. This region, encompassing parts of Europe, Africa, and Asia, is particularly vulnerable, due to its complex interplay of mid-latitude and subtropical weather systems and its distinctive geographical features, such as mountain ranges and extensive coastlines.

The region's vulnerability to air pollution is exacerbated by unsustainable development, urbanization, and industrialization, underscoring the need for continued research and policy interventions. The impacts of Ozone, CO, CO_2, NO, NO_2, and other pollutants have been extensively studied by researchers [29,30]. However, atmospheric radon remains mostly unexplored. The general belief that oceanic masses serve as a sink for natural radioactivity has deviated the interest of the scientific community towards mainland regions. Nevertheless, recent studies have found hazardous concentrations of radon indoors in many Mediterranean locations, even when local radon fluxes are low [31–33]. Therefore, the monitoring of atmospheric radon is important, even for coastal and insular sites. While radon concentrations in open air are generally harmless, inadequate ventilation indoors can lead to carcinogenic levels.

This paper presents the findings of a 12-year study on radon conducted from January 2011 to December 2022 at the Giordan Lighthouse station on the island of Gozo, Malta. Located in the Central Mediterranean, Gozo's strategic position enables effective monitoring of air mass movements between Africa and Europe (from south to north) and between Europe and Central Asia (from west to east). Our research involves an analysis of seasonal and diurnal variations in radon levels, alongside analysis of relevant meteorological variables, clustering of air mass back trajectories, and assessment of local and remote radon production. The findings provide critical insights into the dynamics of atmospheric radon, which are significant not only for the Maltese islands, but also for enhancing our

understanding of transcontinental radon transport in the Central Mediterranean, a region that has remained largely unexplored.

2. Materials and Methods

2.1. Monitoring Site

Gozo, the second-largest island in the Maltese archipelago after Malta, boasts a population of approximately 29,000 inhabitants, and sustains its economy primarily through agriculture and tourism. Positioned approximately 100 km south of Sicily and 400 km from the North African coast, Gozo finds itself centrally situated in the Mediterranean, halfway between the Suez Canal and Gibraltar, as well as between Sicily and the North African coast (Figure 1).

The Giordan Lighthouse (GLH), located on Gozo at coordinates 36.4°24′ N, 14.13°09′ E, and at an altitude of 160 m above sea level, was designated a Global Atmosphere Watch (GAW) station in 2001. Subsequently, it underwent full-fledged station upgrades in 2010, courtesy of funding from the European Regional Development Fund (ERDF), allocated to Malta following its accession to the European Union.
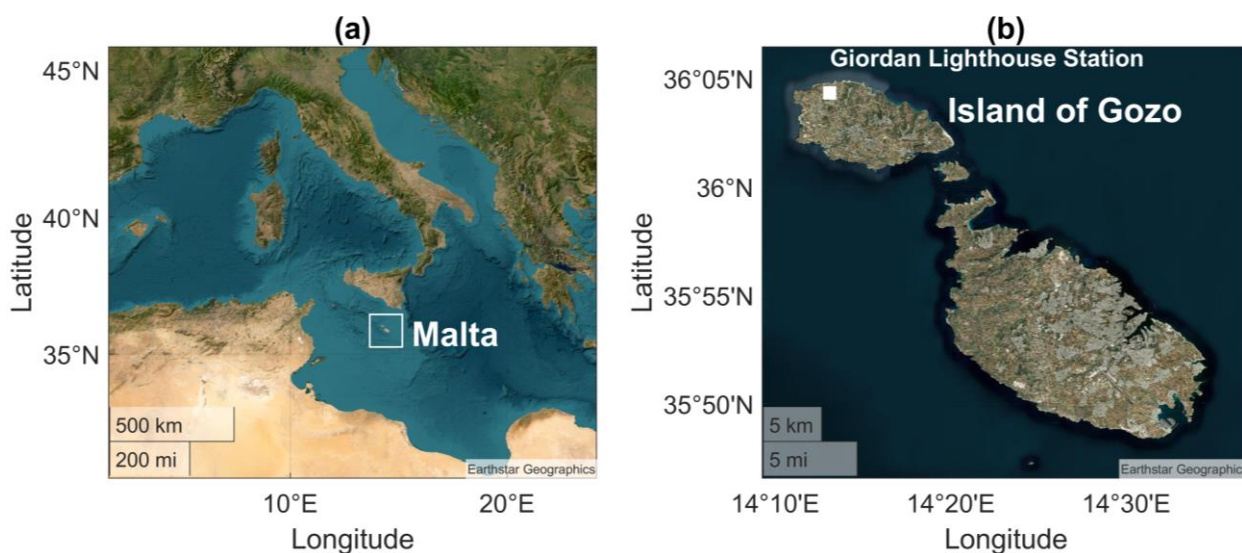

Figure 1. The geographical location of the monitoring site at the Giordan Lighthouse (GLH) on the island of Gozo, Malta: (**a**) the global location of Malta and (**b**) the local location of the GLH.

2.2. Monitoring Equipment

The instrument used for radon measurement was the Tracerlab Radon Daughter Monitor Automatic Step-Filter System (Tracerlab, Köln, Germany, model RDM-PLUS-SF), a specialized detector employed at various Global Atmospheric Watch (GAW) stations. This device operates with a support pump that draws ambient air onto a PTFE (polytetrafluoroethylene) filter tape, facilitating the indirect quantification of radon through Potential Alpha Energy Concentration (PAEC), by an algorithm embedded in the instrument. The decay of radon generates a series of short-lived radioactive isotopes, such as Po-218, Pb-214, Bi-214, and Po-214. PAEC captures the biological impact of this collection of decay products, representing the total alpha energy emitted from all decay products within a specified volume until complete decay occurs.

Prior to installation at the GLH station, the device was calibrated by the manufacturer and supplier, Tracerlab, Germany. Upon becoming operational, atmospheric radon measurements were carried out bi-hourly using the "Continuous Slow Method". This method allows for simultaneous sampling and analysis of data, facilitating the collection of long-term, real-time measurement results and providing radon concentration data for specified

time intervals. The measurement cycle commenced on even hours, featuring a counting interval of 2 h per measurement and an airflow rate of 600 L/h. Each cycle consisted of 24 measurements, prompting the instrument to change filters every 48 h to initiate a new cycle. The detector's performance is contingent upon the sampling method, volume, and duration. The lower limit of detection was 0.1 Bqm^{-3}, with detection efficiency and uncertainty at 20% and 10% (k = 1), respectively, under the specified conditions.

Wind direction and speed were measured using a traditional vane and cup anemometer (Lambrecht, Germany, model 14,512). This anemometer records wind direction within a range of 0 to 360°, and wind speed from 0 to 35 ms^{-1}. Starting from the year 2021, the wind anemometer was replaced with a new instrument utilizing ultrasonic technology (Lufft, Fellbach, Germany, model WS200), extending the wind speed measurement range up to 75 ms^{-1}.

Additionally, meteorological data from Malta's sole climate station (WMO: 16.597) were obtained from NOAA. The data, standardized in METAR and SYNOP formats as defined in WMO Pub. 306 Sections FM 15 and FM 12, respectively, include timestamps, along with wind speed and direction, temperature, dew point, and air pressure. The merged sub-hourly dataset spanning 2011–2022 comprised 10 m wind speed information (ms^{-1}) sourced from both data repositories for the current analysis.

Air temperature and relative humidity were measured using a probe (Vaisala, Finland, model HMP60). This probe captures temperature within a range of −40 to 60 °C, and relative humidity from 0 to 100%. Equipped with a platinum resistance temperature (PRT) detector and a Vaisala INTERCAP® (Toronto, Canada) capacitive relative humidity sensor, the HMP60 probe ensures precise measurements.

2.3. Dataset Overview

As previously discussed, atmospheric radon primarily originates from geological sources, with critical factors such as the mineralogical composition of bedrock (containing uranium), soil characteristics, and meteorological conditions governing its emanation, migration, and exhalation into the atmosphere. Given the essentially constant nature of mineralogical and soil variables throughout the study period (from 2011 to 2022), the present work is focused on the assessment of radon concentrations in relation to both local and remote radon production, as well as the key meteorological parameters that influence the release of radon from the soil into the atmosphere and the transportation of radon between different geographical territories.

All variables under examination were continuously monitored from January 2011 to December 2022, spanning 4383 days. Radon levels were measured every two hours, while wind direction (WD), wind speed (WS), air temperature (AT), and relative humidity (RH) were recorded hourly. Hourly radon values were derived through linear interpolation to enhance the resolution of different composites and align more closely with meteorological variables. The measurement units are Becquerels per cubic meter (Bqm^{-3}) for radon, degrees (deg) for wind direction, meters per second (ms^{-1}) for wind speed, Celsius (°C) for air temperature, and percentage (%) for relative humidity. The time is expressed in hours, according to the local time of Malta, in a 24 h format.

Table 1 presents a summary of the key statistical parameters derived directly from the validated raw measurements.

Table 1. Significant statistics of radon and meteorological variables.

Variable	Acronym	Units	Mean	Standard Deviation	Maximum	Minimum	10th Percentile	90th Percentile
Atmospheric radon-222 concentration	Radon	Bqm^{-3}	2.16	1.62	26.70	0.10	0.70	4.15
Wind direction	WD	deg	213.5	92.3	353.3	0.0	70.5	312.8
Wind speed	WS	ms^{-1}	8.2	4.9	42.8	0.0	2.9	15.2
Air temperature	AT	^{o}C	19.4	6.2	52.9	−6.1	12.1	27.5
Relative humidity	RH	%	70.5	14.2	100.2	0.5	51.4	87.4

The WS data for the years 2017 to 2020 required correction due to a malfunction in the anemometer, resulting in erroneous measurements on specific dates. To rectify this issue, WS data from the nearby WMO climate station in Luqa, Malta, were utilized. The suitability of this reference dataset was confirmed through monthly and daytime WD statistical plots, and the correction process involved the application of the Least Square Method.

3. Results and Discussion

3.1. Seasonal Composite

Analysis of the multi-year radon time series reveals a consistent seasonal pattern, with elevated concentrations during the summer months (June, July, August) and fall (September, October, November), and lower concentrations in winter (December, January, February) and spring (March, April, May). Notably, peak concentrations are typically observed from August to September, while the lowest levels are recorded from December to March.

The seasonal variation in radon levels at both inland and coastal monitoring sites is driven by changes in the local radon production and importation. The amount of imported radon is determined by the interplay between oceanic and terrestrial radon sources, which are largely affected by seasonal meteorological changes, particularly wind direction. Given that oceanic radon production is relatively minimal compared to terrestrial sources, periods of low radon concentration are often observed when oceanic fetch dominates, resulting in minimal radon importation. In contrast, notable increases in baseline radon levels are typically attributed to the influence of remote land sources.

At insular locations like the GLH station, the interplay between oceanic and terrestrial influences remains significant throughout the year. Therefore, the seasonal patterns should be analyzed at different timescales to identify the rapid fluctuations between high and low radon concentrations.

On a monthly timescale, the complete dataset of radon values is organized by month, and the mean, together with the 90th and 10th percentiles, is calculated for each monthly subset. Within this time frame, the annual evolution of radon levels measured at the GLH station shows a clear seasonal pattern, yet is characterized by significant and stable standard deviation of the mean values, and high inter-monthly variability in all three statistics. The amplitude of the cycle is particularly pronounced for the highest values indicated by the 90th percentile, with monthly mean values ranging from a minimum in February to a maximum in August. This trend suggests a shift towards an increased terrestrial influence in late summer and early autumn and a decrease in winter, highlighting its strong seasonal dependence (Figure 2a).

Conversely, the 10th percentile values show two distinct terms: during the cold season (from December to March), these values remain remarkably stable and low (around 0.5 Bqm^{-3}), while during the warm season (from June to September), they gradually increase, reaching their monthly average (around 1.0 Bqm^{-3}). Therefore, the 10th percentile

values serve as a baseline for the radon concentration in Gozo, reflecting a predominantly local production and the oceanic origin of any imported radon concentration during the cold season (Figure 2a).

On a daily timescale, radon values are aggregated by "day of the year" (ranging from day 1 to day 365; leap year extra days are excluded), and the mean and percentiles are calculated for each individual day. Within this timeframe, the seasonal pattern is less evident as the amplitude of radon variation increases, particularly for the highest values. Notably, some radon peaks occur outside of the anticipated seasonal ranges. This analysis highlights the interaction between oceanic and terrestrial influences on the radon concentrations measured in Gozo, indicating the need for a thorough examination of all contributing variables for an accurate characterization (Figure 2b).
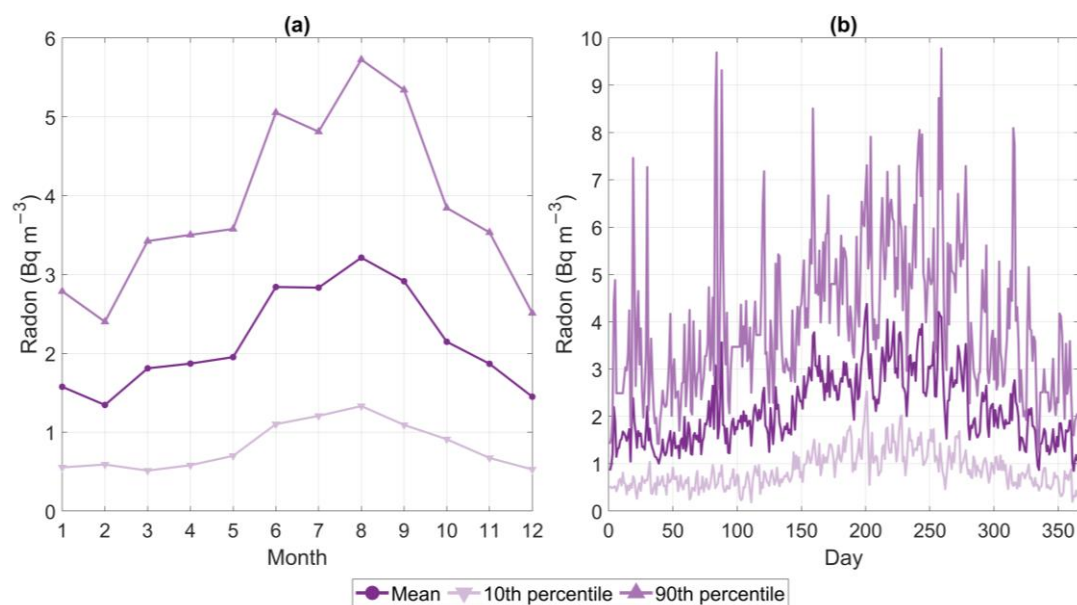

Figure 2. Seasonal composite of radon. Mean, 10th, and 90th percentile values: (**a**) monthly timescale and (**b**) daily timescale. Standard deviation is 1.46 Bqm⁻³ and 1.23 Bqm⁻³ for monthly and daily scales, respectively. Whiskers are excluded in subplot "b" for visualization purposes.

Given the high-frequency fluctuations in radon levels, climate variables are examined on both monthly and daily timescales, with mean values supplemented by the 10th and 90th percentiles. WD varies seasonally due to shifts in the geographical origin of incoming winds, with differences of up to 50 deg. The mean WD oscillates around 213° (Figure 3a1), approximating the geographical southwest (SW). However, this mean direction does not necessarily reflect the predominant wind direction in Gozo, but rather the average of multiple recorded wind directions. On a daily timescale, the 90th percentile values indicate a constant presence of winds from approximately 310°, near the northwest (NW), while the mean and 10th percentile values show significant variation, representing a range of directions from 27° to 280°, spanning from the northeast (NE) to the NW (Figure 3a2).

WS and AT exhibit clear seasonal variations with inverse maxima, influenced by Malta's Mediterranean climate, characterized by high temperatures and low wind speeds in summer, and the opposite in winter (Figure 3b1,b2,c1,c2).

RH shows a clear relationship with WD, with lower values associated with winds from the NE (Figure 3d1). Considering Gozo's geographical location, northerly winds predominantly originate from terrestrial regions as they traverse Europe, potentially resulting in lower local humidity levels compared to southerly winds, which are more

influenced by the Mediterranean Sea. On a daily timescale, RH shows 90th percentile values that increase in summer, reflecting the mix of WD and the alternating incidence of dry and humid winds (Figure 3d2). The role of local radon sources, evaluated in the following sections, will aid in accurately describing the RH trend.
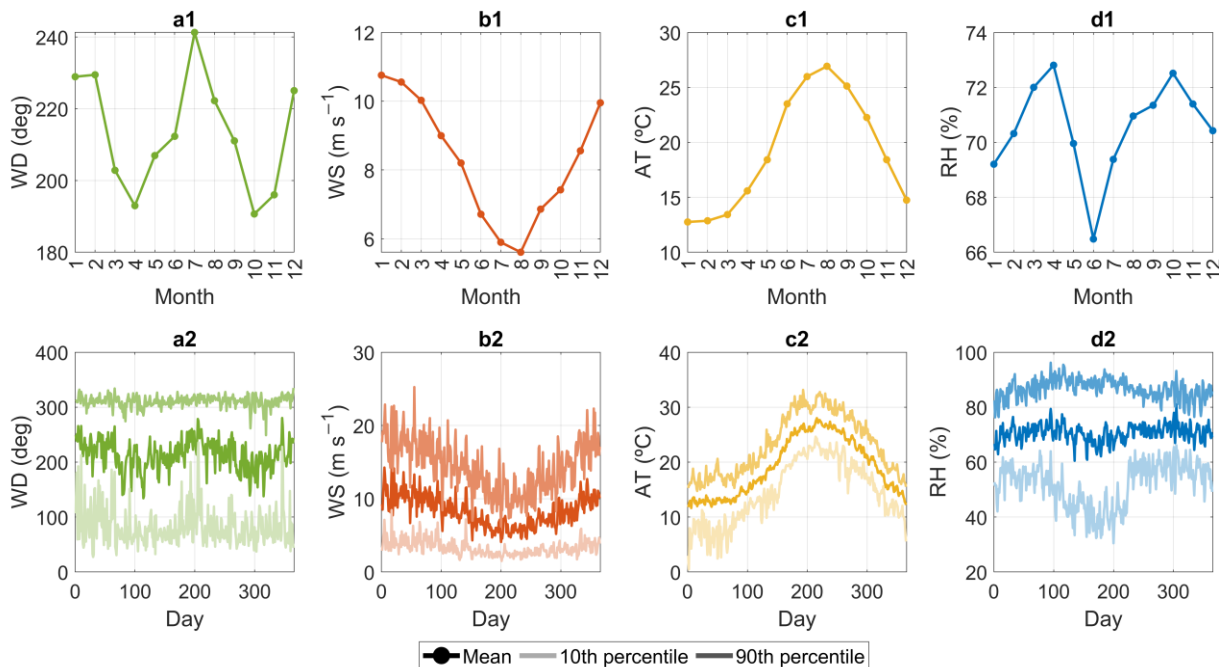

Figure 3. Seasonal composite of meteorological variables. Mean values and mean, 10th, and 90th percentile values at monthly and daily timescales, respectively: (**a1**,**a2**) WD, (**b1**,**b2**) WS, (**c1**,**c2**) AT, and (**d1**,**d2**) RH.

The seasonal radon histograms present a lognormal distribution, accounting for an accumulation of values around a low average, and a long tail of high, though infrequent, values (Figure 4a). As expected, radon accumulation is more significant in summer (Figure 4a2). However, isolated radon peaks are attained in fall and spring (Figure 4a1,a3).

The WD histograms corroborate the dominance of NW winds across all seasons, with this prevalence particularly pronounced in summer and winter, for which the histograms display almost identical distributions (Figure 4b). This intriguing alignment, despite the seasonal fluctuation of radon (peaking in summer and declining in winter), warrants further investigation through analysis of wind back trajectories, which will be made in Section 3.3. Conversely, the NE and east (E) directions assume a significant secondary position in fall, and especially in spring (Figure 4b1,b3). The total absence of the north (N) component in all seasons is notable, since the interval of wind directions between −15 deg and +15 deg has no representation in any of the WD histograms. This is certainly due to the closeness of Gozo to Sicily and particularly Mt. Etna (3320 m), which blocks the direct arrival of N winds, deviating them towards the NW and NE directions.

Regarding WS, AT, and RH, the histograms indicate minimal distribution variations between seasons, confirming that the previous analyses of mean values sufficiently represent their respective seasonal trends (Figure 4c–e). Notably, summer is characterized by climatic stability, whereas winter exhibits significant instability. Fall and spring serve as transitional periods.
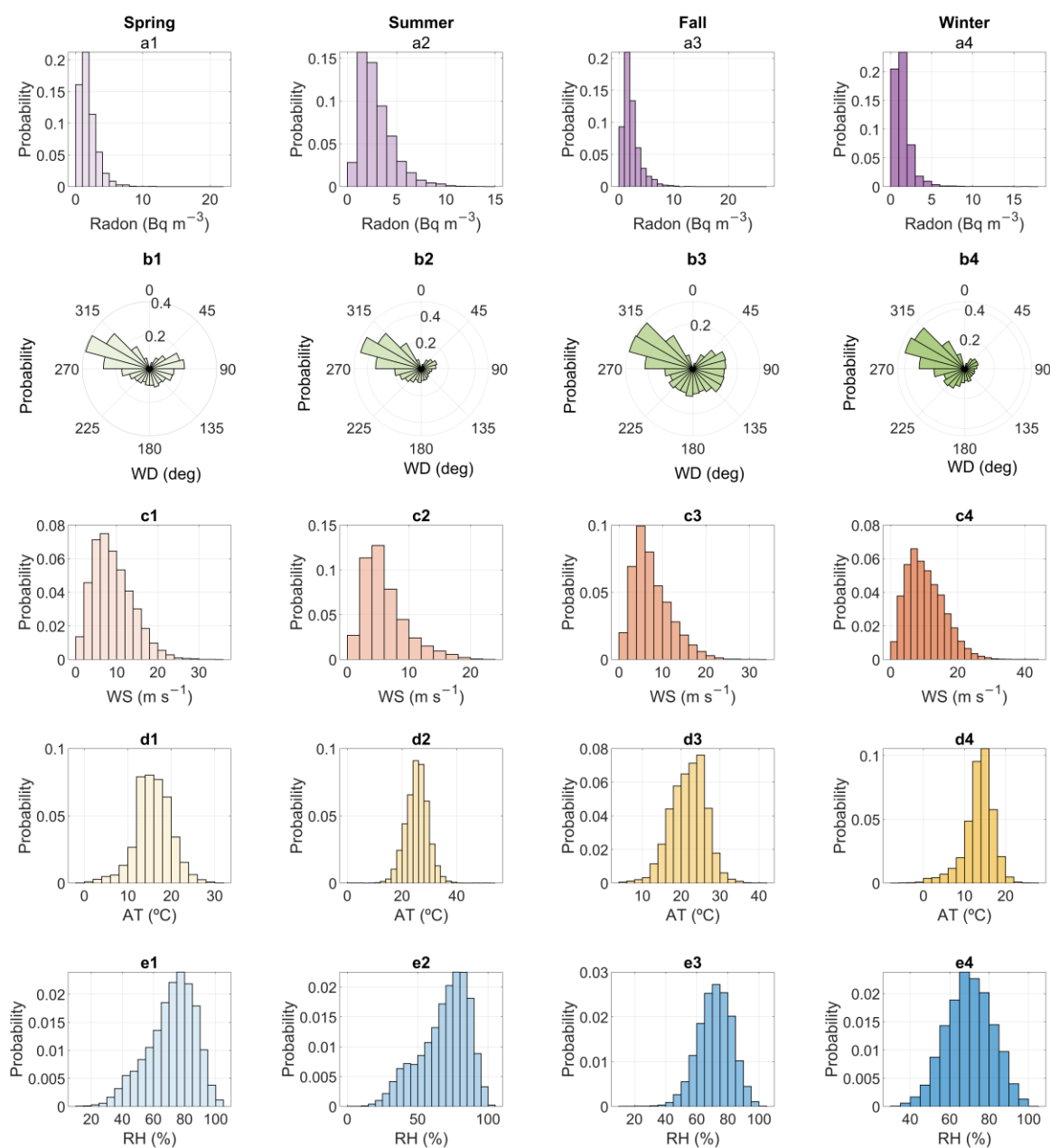
Figure 4. Histograms per season (1 = Spring, 2 = Summer, 3 = Fall, 4 = Winter): (**a1–a4**) radon, (**b1–b4**) WD, (**c1–c4**) WS, (**d1–d4**) AT, and (**e1–e4**) RH.

3.2. Diurnal Composite

At flat inland monitoring sites, the radon concentration varies seasonally, due to changes in radon production (local and remote) and transport associated with seasonal climatic variations. However, radon production and transport remain essentially constant throughout the diurnal cycle, because there are no significant changes in either radon fluxes (local nor remote) nor radon importation (mostly tied to seasonal changes in wind direction).

Consequently, most of the variability in radon concentration observed on sub-diurnal timescales is due to the dilution of locally emitted radon within the atmospheric boundary layer. In such circumstances, diurnal cycles could be computed for each season,

to properly isolate the effects of radon production, importation, and dilution. These cycles present different mean radon values, since seasons most affected by terrestrial fetch will register higher radon concentrations. However, they all share a common sinusoidal profile for a 24 h period, with a maximum around sunrise and a minimum in the early afternoon. Radon accumulates at night, when the local atmosphere is more stable due to the steadiness of the meteorological variables and persistency of low-speed winds. During the day, radon decreases because the atmosphere is more thoroughly mixed due to the elevated gradients of the meteorological variables, and especially the uprise of the wind speed.

In the case of insular and most coastal sites, where there is a constant alternation between oceanic and terrestrial influences, radon importation could vary, even on a daily scale. Therefore, seasonal–diurnal cycles might not be enough to subtract the influence of remote sources, and the regular radon diurnal cycle is altered. On the other side, highly elevated terrains are very much influenced by anabatic and non-anabatic flows, triggered by the diurnal gradients of the meteorological variables.

Studies at the Manua Loa Observatory in Hawaii have identified a diurnal cycle characterized by an early-afternoon maximum, and a midmorning minimum, with maximum almost reached again at sunrise. The diurnal cycle at this high-elevation mountain site can be primarily attributed to anabatic and katabatic flows that bring radon from the island and volcano flanks to the observatory. The longest land fetch (across the island and up the mountain) occurs for the anabatic flow conditions, resulting in the early-afternoon maximum values. Minimum concentrations, most representative of tropospheric air, are seen midmorning, in the lull period between anabatic and katabatic flow conditions [27,34,35].

Investigations at the High Altitude Research Station Jungfraujoch, located in the northwest flank of the Swiss Alps, have also reported maximum radon in the late afternoon as a result of boundary-layer air being brought to the mountain peak by anabatic winds [36]. Profuse vegetation around the monitoring site could also present a singular radon diurnal cycle. A project focused on three large forest areas in Southeast Queensland, Australia, showed a secondary peak of radon concentration in the afternoon due to the release of radon into the atmosphere by plant transpiration at that time [37].

To calculate the seasonal diurnal cycles of the observations recorded at the GLH station, the radon dataset was divided into the four seasons (spring, summer, fall, and winter) and grouped by daytime (24 h, from 00:00 to 23:00) within each season. After this segregation, the mean was calculated for each individual season and daytime (Figure 5a).

As expected from the results of the monthly compilation discussed earlier, the mean diurnal values show high concentrations in summer and fall, in contrast to low concentrations in spring and winter (Figure 5a).

The differences between the seasonal daily radon amplitudes are relatively small compared to those typically observed at mainland sites, which is due to the mixture of oceanic and terrestrial fetch in Gozo. However, the superior amplitude of summer and fall highlights the predominant presence of terrestrial fetch, conveyed and installed by the low-speed winds of the warm months that allow for the accumulation of radon in the lack of turbulences.

Regarding the different radon diurnal cycles, summer is characterized by a morning maximum around 09:00 (all times are in hours, local time), which rapidly decreases towards noon, when radon reaches a minimum. In the afternoon, radon rises rapidly until sunset around 19:00, when the value is again close to the maximum, and remains stable during the night. After sunrise, radon accumulates for a few hours and peaks in the morning, when the cycle begins again (Figure 5c).

In fall, spring, and winter, the morning radon peak gradually disappears, and radon levels become increasingly unstable at night. The radon minimum is still reached around

noon (between 12:00 and 14:00), and the only maximum occurs in the evening (between 18:00 and 20:00) (Figure 5b,d,e).
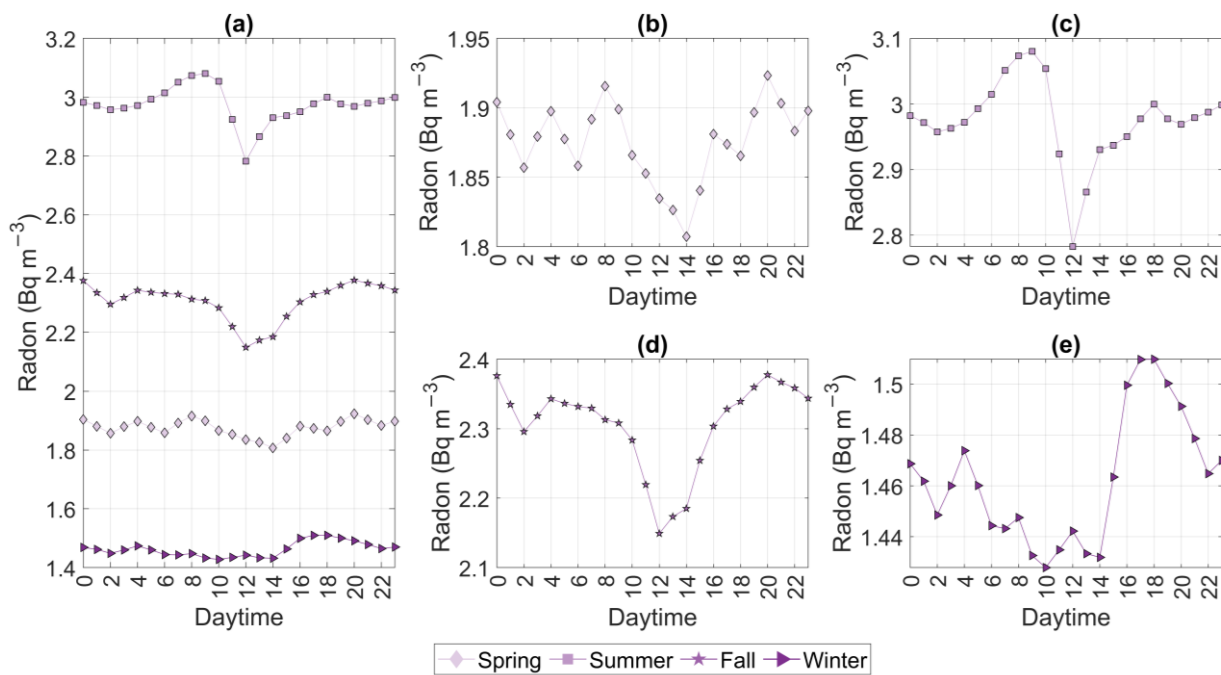

Figure 5. Radon diurnal composite per season: (**a**) all seasons, (**b**) spring, (**c**) summer, (**d**) fall, and (**e**) winter. Subplots (**b–e**) provide insight into seasons individually for better scaled representation of diurnal evolution of radon. Standard deviations are 1.37 Bqm^{-3}, 1.73 Bqm^{-3}, 1.70 Bqm^3, and 1.21 Bqm^{-3}, and daytime standard deviations differ by less than 11%, 10%, 13%, and 18% compared to their seasonal values for spring, summer, fall, and winter, respectively.

The diurnal cycle of WS, AT, and RH is similar in all seasons, revealing strong advection and vertical mixing in the daytime, and the formation of a thermally stabilized structure of the atmosphere in the night-time. The values are constant at night, showing enhanced steadiness of the local atmosphere (Figure 6b–d). After sunrise, all meteorological variables evolve to their daytime values due to solar radiation, so their gradients are elevated, especially around midday, when the most extreme observations are registered. WD shows a similar cycle, even though it is not a thermally driven variable (Figure 6a).

Seasonal differences affect the mean values of the variables, the amplitude of the cycles, and the stability of the profile during the daytime. Summer exhibits greater gradients and more stable values. In fall, spring, and winter, both amplitudes and stability decrease. The seasonal differences in the diurnal cycle of the wind are of special interest, since they have a direct effect on radon importation and radon accumulation. WD clearly turns to the north after sunrise in summer, and WS is low, with a substantial gradient towards midday. However, WD is mostly constant in winter, and WS is consistently high all day, with just a small fluctuation around midday.
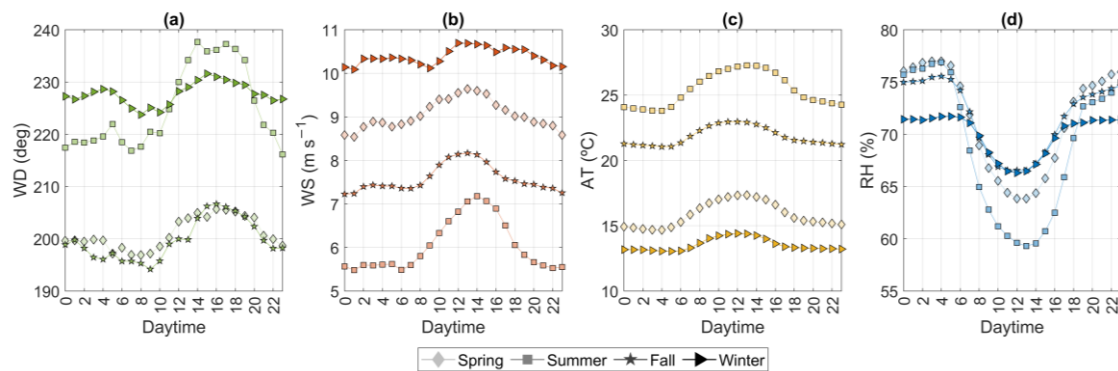
Figure 6. Diurnal composite of meteorological variables per season: (**a**) WD, (**b**) WS, (**c**) AT, and (**d**) RH.

Following the examination of the individual seasonal–diurnal cycles, the morning radon maximum and midday minimum can be attributed to the conditions of the local atmosphere, which is stable at night and increasingly mixed during daylight. However, the secondary radon maximum observed in the late afternoon and evening might not be due to local atmospheric conditions. Typically, air turbulence peaks in the midafternoon, which would usually result in lower radon concentrations at this time. The shift in the wind towards the N during daylight hours, particularly in the afternoon, increases the terrestrial fetch, likely causing this late secondary maximum (Figure 6a). Additionally, the measurement equipment is situated at over 160 m above sea level on a hill near the coast (Figure 1b). The alternation between anabatic and katabatic winds, driven by gradients in wind speed, air temperature, and relative humidity, could contribute to the evening rise in radon levels, as extensively reported in studies at mountain sites [35,36].

3.3. Air Mass Back Trajectory Analyses

To understand the influence of air mass transport on atmospheric radon levels at the GLH station, back trajectory and clustering analyses were conducted, alongside radon measurements. These analyses sought to identify the specific regions of radon importation into Gozo, to complement the possible main geographical sector already underlined by the seasonal evolution of radon and meteorological variables.

Trajectories and clusters were calculated using the PC version of the HYSPLIT v5 model developed by NOAA/ARL [38–40], fed by the GDAS (Global Data Assimilation System) one-degree archive produced by the National Centers for Environmental Prediction (NCEP) as part of their Global Data Assimilation System. This archive contains global climate data that have been assimilated from various sources, including satellite observations, surface measurements, and upper-air measurements, to produce a comprehensive and consistent set of atmospheric data. The GDAS one-degree archive is widely used for a variety of applications, including weather forecasting, climate research, and air quality modeling, as it provides high-quality, global atmospheric data (Global Data Assimilation System, 2020)

As a radioactive element, radon undergoes exponential decay, with a half-life of 3.83 days, and a 92% reduction in its initial activity over a 14-day period. Most studies concerning atmospheric radon focus on back trajectories spanning 4 to 7 days, when most of the radioactivity of the gas is delivered, so the primary fetch regions are highlighted. However, in this work, 7-day and 14-day back trajectory analyses were performed to identify potential secondary, more distant locations of influence, and to enhance the comprehension of the primary ones. Given the mixed oceanic and terrestrial fetches typical of the island territory, the complex profile of wind direction year-round, and the presence of

seasonal, very differential low- and high-speed winds, this dual analysis was deemed pertinent.

In both cases, trajectory analyses were conducted for the entire 2011–2022 study period (4383 days), and merged into four cluster trajectories after comparing the results based on two, three, four, and five cluster trajectories. While some trajectories could be merged due to similarities in coordinates or low incidence, this number of cluster trajectories enables a detailed analysis of the primary wind sources, which is crucial after revealing the complexity of the wind direction profile.

Based on the 14-day back trajectory analysis, seasonal plots of cluster trajectories show more distant sources in winter, fall, and spring (Figure 7a,c,d), due to the prevalence of high-speed winds, which can reach Gozo from more remote locations within 14 days, compared to summer, when low-speed winds dominate (Figure 7b). These longer trajectories imply greater oceanic contact as they traverse the Atlantic Ocean before crossing Europe, explaining the prevalence of oceanic fetch in colder months, even under the massive presence of NW air fluxes. Conversely, the shorter trajectories of the summer winds primarily interact with the European continent, contributing to the terrestrial fetch observed during warmer months.
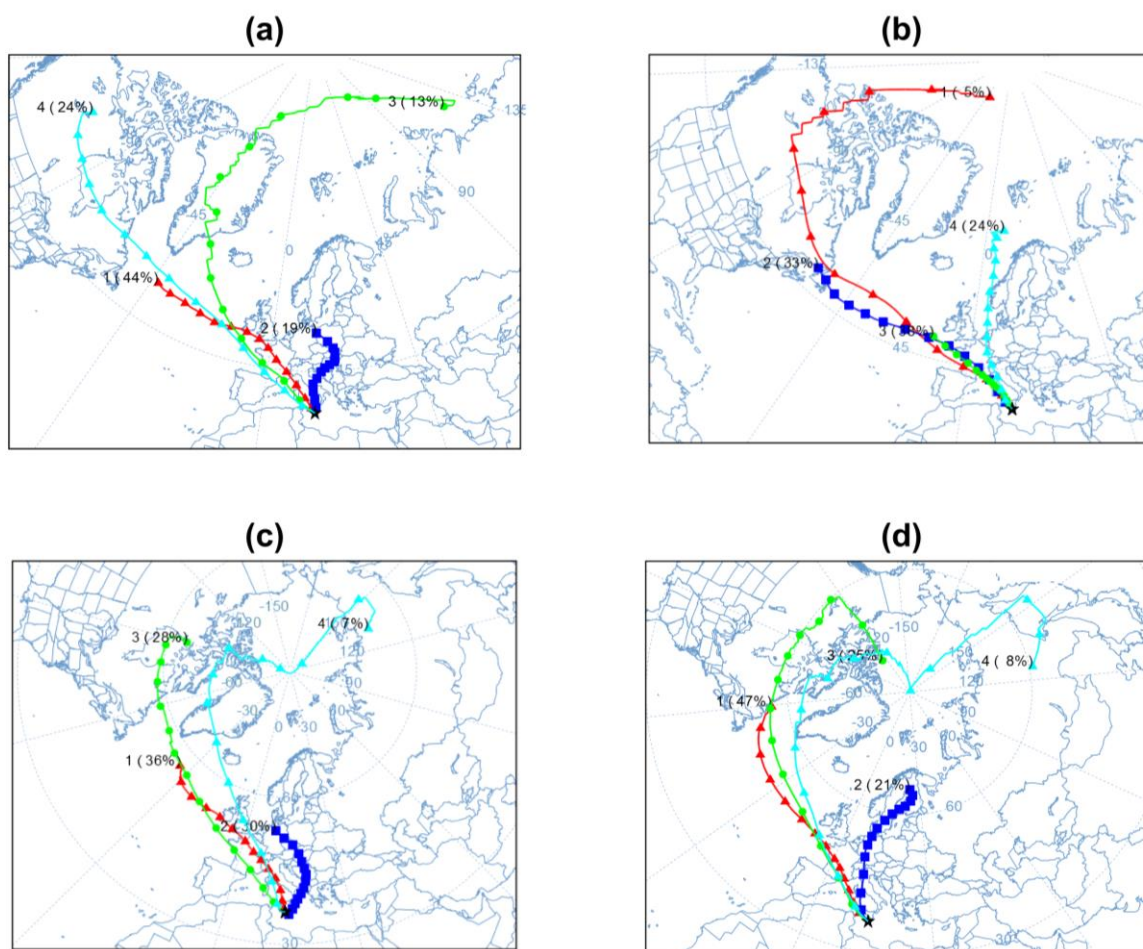

Figure 7. Air mass source clustering based on Hysplit 14-day back trajectories (markers every 24 h): (**a**) spring, (**b**) summer, (**c**) fall, and (**d**) winter. Colors are automatically assigned and solely represent different cluster trajectories.

The 7-day back trajectory analysis provides details of the contribution of each cluster (Figure 8). In summer, NW winds are highly in contact with the Pyrenees, the frontier between Spain and France, and Mt. Albo in Sardinia (trajectories 1 and 3), whereas N and

NE winds are mostly in contact with the Apennines and Mt. Etna in continental Italy and Sicily, respectively (trajectories 2 and 4), and the Alps in Central Europe (trajectory 4). These mountain ranges are the most prominent radon producers in Europe, as is concluded in the following Section 3.4, and they could be pointed out as responsible for the high radon concentrations measured at the GLH station in this season. The influence of Mt. Etna is crucial, due to its proximity to Gozo and its volcanic activity [41,42]. On the contrary, such winds are neglected in winter, when the NW direction dominates (Figure 8d).

The fall winds mostly come from the NW, passing again through Pyrenees, Alps, Sardinia, and Sicily, but to a lower extent, due to the increment in the contribution of the Atlantic Ocean (trajectory 2 and 4). There is also a significant NE component in the wind, but it is totally spread over the Mediterranean Sea (trajectory 2). This composition would explain the still-high concentration of radon in this season, although this concentration is lower than in summer.

During spring, the winds exhibit reduced continental interaction, but continue to transport radon from regions such as the Pyrenees, the Alps, and Sardinia (trajectories 2, 3, and 4). Additionally, there is a significant contribution from the Balkans (trajectory 1). This dynamic could account for the still-elevated radon concentrations during this season, although these concentrations are lower and less stable compared to those in summer and fall.

In winter, winds show minimal interaction with Sicily and the Balkans. Their continental influence is primarily confined to the Pyrenees and Sardinia (trajectories 3 and 4), and the Alps (trajectory 2). In contraposition, the most significant contribution arrives from the Atlantic Ocean (Figure 8d).

According to both 14-day and 7-day back trajectories, radon importation from African and Asian continents is neglectable throughout the year, since the presence of long-term southerly and pure westerly winds is minimal, and does not have clustering representation.
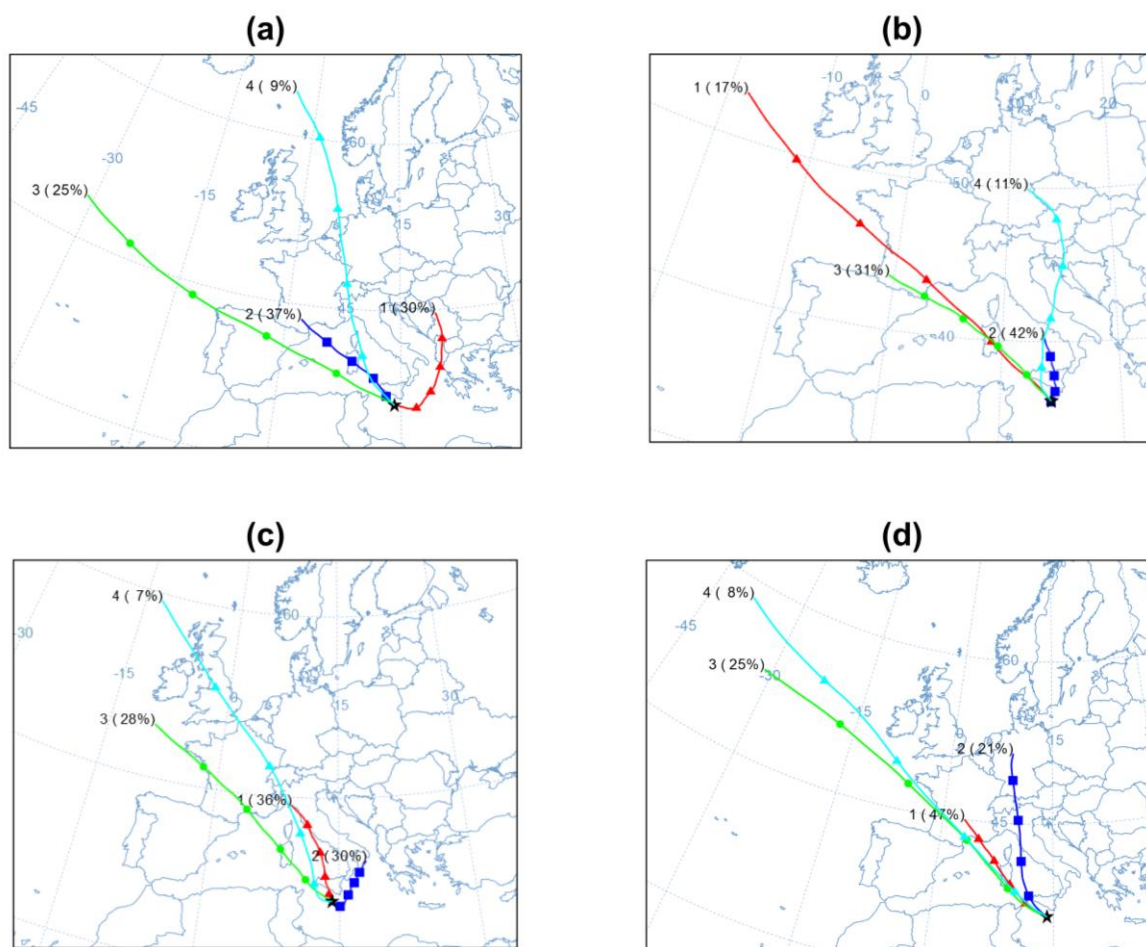
Figure 8. Air mass source clustering based on Hysplit 7-day back trajectories (markers every 24 h): (**a**) spring, (**b**) summer, (**c**) fall, and (**d**) winter. Colors are automatically assigned and solely represent different cluster trajectories.

3.4. Radon Production Assessment

As previously stated, the local radon concentration is a function of radon production, both local and remote, and meteorological variables, whose seasonal dynamics influence radon release and transportation.

The production of radon in each region is primarily determined by the geological composition of the area. The Maltese islands sit atop two predominant stratigraphic formations. The Lower Coralline Limestone, the older and harder of the two formations, forms the bedrock of the islands. Overlying this formation is the Globigerina Limestone, a softer, finer-grained limestone subdivided into the Lower, Middle, and Upper Globigerina members [43–45]. Due to the low uranium concentrations in these rock compositions, the self-production of radon at the monitoring site is minimal. This assumption is supported by uranium in soil maps and radon flux maps developed by the Radioactivity Environmental Monitoring section of the Joint Research Centre of the European Community [46,47].

As underlined by the back trajectory analyses (Section 3.3), radon arriving in Gozo mainly comes from north and west Europe. Therefore, the radon production of the European continent is essential for understanding the radon concentrations measured at the GLH station.

Monthly radon flux maps of the European Union are accessible through the "traceRadon" project and database [48]. Utilizing this resource, the European average radon flux

per season was calculated for the period under evaluation in this study (2011–2022). The resulting maps (Figure 9) illustrate that European radon production peaks in summer (Figure 9b), followed by fall (Figure 9a) and spring (Figure 9c), and reaches its minimum in winter (Figure 9d), when soil freezing leads to a decay in radon exhalation. The primary European radon sources are situated in the mountain ranges of Portugal, Spain, Sweden, Italy, and France, where the Cantabrian Mountains, Pyrenees, Scandinavian Mountains, Mt. Albo, Apennines, and Mt. Etna are the main formations.

This radon production overview is totally compatible with the outcomes of the seasonal composite and back trajectory analyses exposed in the previous sections (Sections 3.1 and 3.3).
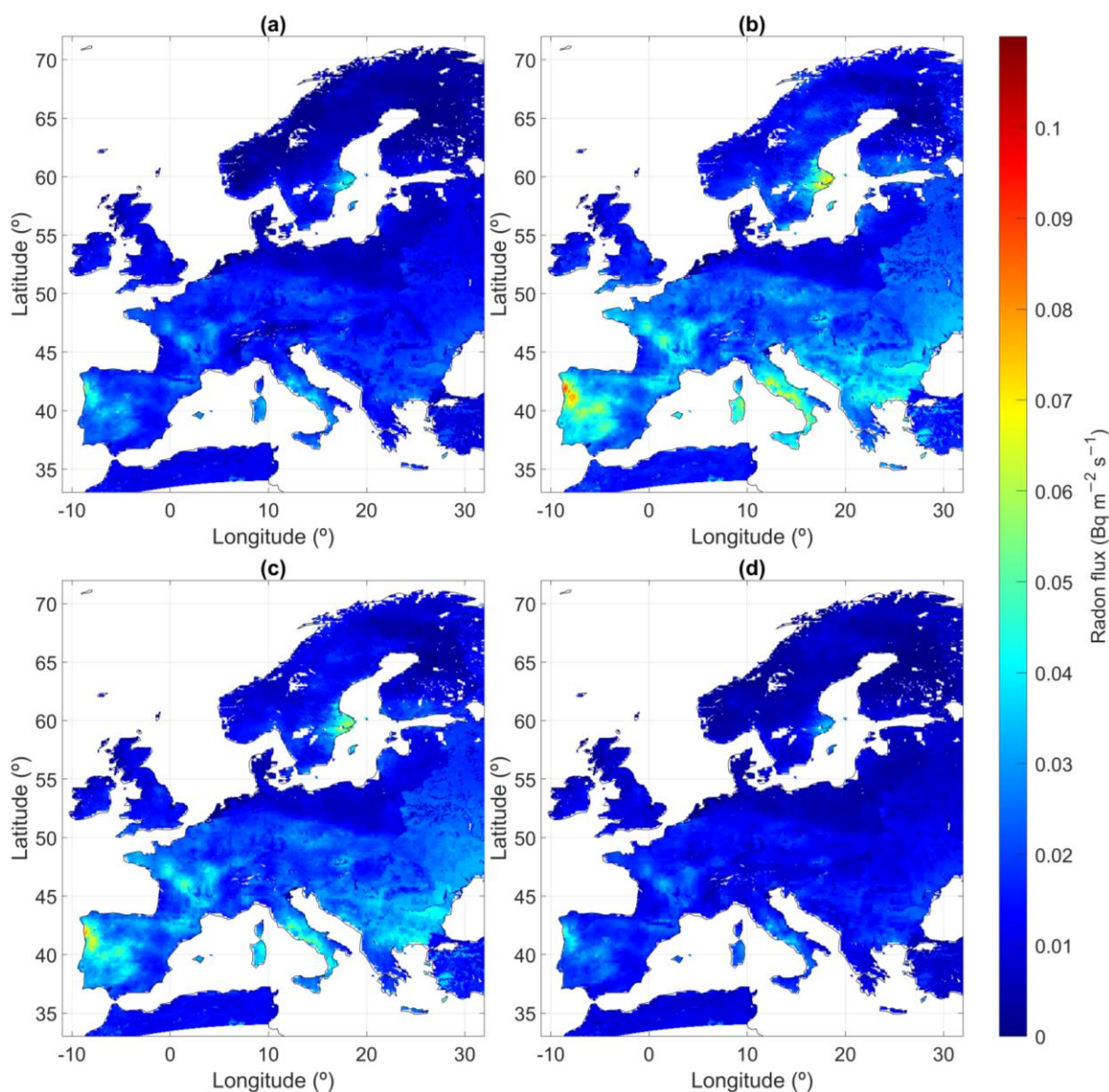
Figure 9. Seasonal radon flux maps calculated from monthly results published by "traceRadon" during period of the study (2011 to 2022): (**a**) spring, (**b**) summer, (**c**) fall and (**d**) winter.

4. Conclusions

At the GLH station on the island of Gozo, Malta, atmospheric radon is a blend of oceanic and terrestrial influences, owing to its insular location. The distinct seasonal pattern and significant amplitude of radon variation on the monthly scale are indicative of periods of predominantly land or oceanic influence. However, high-frequency

fluctuations detected on the daily scale demonstrate a constant mixture of both origins across the year. In this context, the 10th and 90th radon percentiles may represent primarily oceanic and terrestrial fetches, respectively. The 10th radon percentile values indicate a constant oceanic influence in winter and early spring (December, January, February, and March), gradually transitioning to a mix of oceanic and terrestrial sources for the remainder of the year, in line with trends of the mean and 90th percentile values. Conversely, fluctuations in the 90th radon percentile values show an increase in terrestrial influence during summer and early fall (June, July, August, and September), when it peaks in dominance, and a decline in winter, heavily influenced by seasonal variations.

Seasonal radon composites result from the interplay of radon production (local and remote) and meteorological variables (which impact radon release and transportation) at the monitoring site. The low radon flux at the GLH station, due to the nature of Maltese soil and the moderate Central Mediterranean climate, tends to remain stable, and monthly radon variations can be attributed to imported radon fluctuations. Maximum radon levels are observed in late summer and early autumn, coinciding with increased radon emissions from European sources prior to the onset of winter frost. In these months, NW and NE low-speed winds transport radon from the Pyrenees and Mt. Albo, and the Apennines and Mt. Etna, respectively. The influence of Mt. Etna is crucial, due to its proximity to Gozo and its volcanic activity. Conversely, minimum values are recorded in winter and spring, as European radon flux decreases. Additionally, winds mainly come from the NW, so the contribution from continental Italy and Sicily is annulated. Instead, the increase in wind speed places the origin of most air masses in the Atlantic Ocean, raising the oceanic fetch and therefore further reducing the importation of radon. Radon importation from African and Asian continents is neglectable throughout the year, since the presence of long-term southerly and pure westerly winds is minimal. These season findings support the theory that much of the geogenic natural radiation, which could be taken as a tracker of general air pollution, is transported from Europe to the Mediterranean Basin, influencing regions in Southwestern Europe, North Africa, and the Middle East.

On the diurnal scale, the radon cycle exhibits a morning radon maximum and a midday minimum, attributed to the conditions of the local atmosphere, which is stable at night and increasingly mixed during daylight. There is also a secondary daily maximum registered in the late afternoon and evening, caused by the turn of the wind towards the N direction in the afternoon, which would increase the terrestrial fetch and cause the vespertine high radon values. On the other side, the location of the GLH station, at the top of a hill by the coast, and the alternance between anabatic and katabatic winds, triggered by the gradients of wind speed, air temperature, and relative humidity, could also lead to a vespertine increment of radon. The cycle is well defined in summer, when the conditions at night are very steady, and solar irradiation generates higher gradients in the meteorological variables. However, fluctuations in daily radon are very mild in winter, and a morning maximum is particularly attenuated, because wind speed is high all day through, and solar irradiation is soft, causing turbulence in the local air, even at night-time.

References

1. Wexler, P.; Anderson, B.D. *Encyclopedia of Toxicology*; Academic Press: Cambridge, MA, USA, 2005; Volume 1, ISBN 0127453547.

2. Zahorowski, W.; Chambers, S.D.; Henderson-Sellers, A. Ground Based Radon-222 Observations and Their Application to Atmospheric Studies. *J. Environ. Radioact.* **2004**, *76*, 3–33.

3. Zhang, K.; Feichter, J.; Kazil, J.; Wan, H.; Zhuo, W.; Griffiths, A.D.; Sartorius, H.; Zahorowski, W.; Ramonet, M.; Schmidt, M. Radon Activity in the Lower Troposphere and Its Impact on Ionization Rate: A Global Estimate Using Different Radon Emissions. *Atmos. Chem. Phys.* **2011**, *11*, 7817–7838.

4. IAEA. Sources and Measurements of Radon and Radon Progeny Applied to Climate and Air Quality Studies. *Trends Anal. Chem.* **2012**, *10*, 15–26.

5. Chen, X.; Paatero, J.; Kerminen, V.M.; Riuttanen, L.; Hatakka, J.; Hiltunen, V.; Paasonen, P.; Hirsikko, A.; Franchin, A.; Manninen, H.E.; et al. Responses of the Atmospheric Concentration of Radon-222 to the Vertical Mixing and Spatial Transportation. *Boreal. Environ. Res.* **2016**, *21*, 299–318.

6. Ćujić, M.; Janković Mandić, L.; Petrović, J.; Dragović, R.; Đorđević, M.; Đokić, M.; Dragović, S. Radon-222: Environmental Behavior and Impact to (Human and Non-Human) Biota. *Int. J. Biometeorol.* **2021**, *65*, 69–83. https://doi.org/10.1007/s00484-020-01860-w.

7. Darby, S.; Hill, D.; Auvinen, A.; Barros-Dios, J.M.; Baysson, H.; Bochicchio, F.; Deo, H.; Falk, R.; Forastiere, F.; Hakama, M.; et al. Radon in Homes and Risk of Lung Cancer: Collaborative Analysis of Individual Data from 13 European Case-Control Studies. *Br. Med. J.* **2005**, *330*, 223. https://doi.org/10.1136/bmj.38308.477650.63.

8. Gesell, T.F. Background Atmospheric 222Rn Concentrations Outdoors and Indoors: A Review. *Health Phys.* **1983**, *45*, 289–302. https://doi.org/10.1097/00004032-198308000-00002.

9. Hassan, N.M.; Hosoda, M.; Ishikawa, T.; Sorimachi, A.; Sahoo, S.K.; Tokonami, S.; Fukushi, M. Radon Migration Process and Its Influence Factors; Review. *Jpn. J. Health Phys.* **2009**, *44*, 218–231. https://doi.org/10.5453/jhps.44.218.

10. Nero, A.V.; Nazaroff, W.W. Characterising the Source of Radon Indoors. *Radiat. Prot. Dosim.* **1984**, *7*, 23–39. https://doi.org/10.1093/rpd/7.1-4.23.

11. Schery, S.D.; Gaeddert, D.H.; Wilkening, M.H. Factors Affecting Exhalation of Radon from a Gravelly Sandy Loam. *J. Geophys. Res.* **1984**, *89*, 7299–7309. https://doi.org/10.1029/JD089iD05p07299.

12. Zoran, M.A.; Savastru, R.S.; Savastru, D.M.; Penache, M.C.V. Temporal Trends of Carbon Monoxide (CO) and Radon (222-Rn) Tracers of Urban Air Pollution. *J. Radioanal. Nucl. Chem.* **2019**, *320*, 55–70. https://doi.org/10.1007/s10967-019-06443-7.

13. Shweikani, R.; Giaddui, T.G.; Durrani, S.A. The Effect of Soil Parameters on the Radon Concentration Values in the Environment. *Radiat. Meas.* **1995**, *25*, 581–584. https://doi.org/10.1016/1350-4487(95)00188-K.

14. Gunby, J.A.; Darby, S.C.; Miles, J.C.; Green, B.M.; Cox, D.R. Factors Affecting Indoor Radon Concentrations in the United Kingdom. *Health Phys.* **1993**, *64*, 2–12. https://doi.org/10.1097/00004032-199301000-00001.

15. Sundal, A.V.; Henriksen, H.; Soldal, O.; Strand, T. The Influence of Geological Factors on Indoor Radon Concentrations in Norway. *Sci. Total Environ.* **2004**, *328*, 41–53. https://doi.org/10.1016/j.scitotenv.2004.02.011.

16. Chambers, S.D.; Williams, A.G.; Crawford, J.; Griffiths, A.D. On the Use of Radon for Quantifying the Effects of Atmospheric Stability on Urban Emissions. *Atmos. Chem. Phys.* **2015**, *15*, 1175–1190. https://doi.org/10.5194/acp-15-1175-2015.

17. Charles, M. UNSCEAR Report 2000: Sources and Effects of Ionizing Radiation. *J. Radiol. Prot.* **2001**, *21*, 83–85. https://doi.org/10.1088/0952-4746/21/1/609.

18. Samet, J.M.; Eradze, G.R. Radon and Lung Cancer Risk: Taking Stock at the Millenium. *Environ. Health Perspect.* **2000**, *108*, 635–641. https://doi.org/10.1289/ehp.00108s4635.

19. Clement, C.H.; Tirmarche, M.; Harrison, J.D.; Laurier, D.; Paquet, F.; Blanchardon, E.; Marsh, J.W. Lung Cancer Risk from Radon and Progeny and Statement on Radon. *Ann. ICRP* **2010**, *40*, 1–64. https://doi.org/10.1016/j.icrp.2011.08.011.

20. Al-Zoughool, M.; Krewski, D. Health Effects of Radon: A Review of the Literature. *Int. J. Radiat. Biol.* **2009**, *85*, 57–69.

21. Appleton, J.D. Radon: Sources, Health Risks, and Hazard Mapping. *Ambio* **2007**, *36*, 85–89.

22. Pearson, J.E.; Jones, G.E. Emanation of Radon 222 from Soils and Its Use as a Tracer. *J. Geophys. Res.* **1965**, *70*, 5279–5290. https://doi.org/10.1029/jz070i020p05279.

23. Chambers, S.D.; Williams, A.G.; Conen, F.; Griffiths, A.D.; Reimann, S.; Steinbacher, M.; Krummel, P.B.; Steele, L.P.; van der Schoot, M.V.; Galbally, I.E.; et al. Towards a Universal "Baseline" Characterisation of Air Masses for High- and Low-Altitude Observing Stations Using Radon-222. *Aerosol Air Qual. Res.* **2016**, *16*, 885–899. https://doi.org/10.4209/aaqr.2015.06.0391.

24. Global Atmosphere Watch. *Global Atmosphere Watch Measurements Guide*; World Meteorological Organization: Geneva, Switzerland, 2001.

25. Kim, W.-H.; Ko, H.-J.; Hu, C.-G.; Lee, H.Y.; Lee, C.K.; Chambers, S.D.; Williams, A.G.; Kang, C.-H. Background Level of Atmospheric Radon-222 Concentrations at Gosan Station, Jeju Island, Korea in 2011. *Bull. Korean Chem. Soc.* **2014**, *35*, 1149–1153.

26. Baskaran, M. *Radon: A Tracer for Geological, Geophysical and Geochemical Studies*; Springer: Basel, Switzerland, 2016.

27. Bu, J.O.; Song, J.M.; Kim, W.H.; Kang, C.H.; Song, S.K.; Williams, A.G.; Chambers, S.D. Temporal Variation of Atmospheric Radon-222 and Gaseous Pollutants in Background Area of Korea during 2013–2014. *Asian J. Atmos. Environ.* **2017**, *11*, 114–121. https://doi.org/10.5572/ajae.2017.11.2.114.

28. Schubert, M. Using Radon as Environmental Tracer for the Assessment of Subsurface Non-Aqueous Phase Liquid (NAPL) Contamination—A Review. *Eur. Phys. J. Spec. Top.* **2015**, *224*, 717–730.

29. Cramer, W.; Guiot, J.; Fader, M.; Garrabou, J.; Gattuso, J.-P.; Iglesias, A.; Lange, M.A.; Lionello, P.; Llasat, M.C.; Paz, S.; et al. Climate Change and Interconnected Risks to Sustainable Development in the Mediterranean. *Nat. Clim. Change* **2018**, *8*, 972–980. https://doi.org/10.1038/s41558-018-0299-2.

30. Palmiéri, J.; Orr, J.C.; Dutay, J.C.; Béranger, K.; Schneider, A.; Beuvier, J.; Somot, S. Simulated Anthropogenic CO_2 Storage and Acidification of the Mediterranean Sea. *Biogeosciences* **2015**, *12*, 781–802. https://doi.org/10.5194/bg-12-781-2015.

31. Kikaj, D.; Vaupotič, J. Effective Doses Due to Outdoor and Indoor Radon at a Mediterranean Site. *Radiat. Prot. Dosim.* **2019**, *187*, 215–219. https://doi.org/10.1093/rpd/ncz155.

32. Stoulos, S.; Ioannidou, A. Radon and Its Progenies Variation in the Urban Polluted Atmosphere of the Mediterranean City of Thessaloniki, Greece. *Environ. Sci. Pollut. Res.* **2020**, *27*, 1160–1166. https://doi.org/10.1007/s11356-019-07051-4.

33. Bochicchio, F.; Forastiere, F.; Farchi, S.; Quarto, M.; Axelson, O. Residential Radon Exposure, Diet and Lung Cancer: A Case-Control Study in a Mediterranean Region. *Int. J. Cancer* **2005**, *114*, 983–991. https://doi.org/10.1002/ijc.20799.

34. Williams, A.G.; Chambers, S.; Griffiths, A. Bulk Mixing and Decoupling of the Nocturnal Stable Boundary Layer Characterized Using a Ubiquitous Natural Tracer. *Bound. Layer. Meteorol.* **2013**, *149*, 381–402. https://doi.org/10.1007/s10546-013-9849-3.

35. Chambers, S.D.; Zahorowski, W.; Williams, A.G.; Crawford, J.; Griffiths, A.D. Identifying Tropospheric Baseline Air Masses at Mauna Loa Observatory between 2004 and 2010 Using Radon-222 and Back Trajectories. *J. Geophys. Res. Atmos.* **2013**, *118*, 992–1004. https://doi.org/10.1029/2012JD018212.

36. Griffiths, A.D.; Conen, F.; Weingartner, E.; Zimmermann, L.; Chambers, S.D.; Williams, A.G.; Steinbacher, M. Surface-to-Mountaintop Transport Characterised by Radon Observations at the Jungfraujoch. *Atmos. Chem. Phys.* **2014**, *14*, 12763–12779. https://doi.org/10.5194/acp-14-12763-2014.

37. Jayaratne, E.R.; Ling, X.; Morawska, L. Role of Vegetation in Enhancing Radon Concentration and Ion Production in the Atmosphere. *Environ. Sci. Technol.* **2011**, *45*, 6350–6355. https://doi.org/10.1021/es201152g.

38. Stein, A.F.; Draxler, R.R.; Rolph, G.D.; Stunder, B.J.B.; Cohen, M.D.; Ngan, F. Noaa's Hysplit Atmospheric Transport and Dispersion Modeling System. *Bull. Am. Meteorol. Soc.* **2015**, *96*, 2059–2077.

39. Stein, A.F.; Rolph, G.D.; Stunder, B.J.B.; Cohen, M.D.; Ngan, F.; Chai, T.; Draxler, R.R. NOAA's HYSPLIT Atmospheric Transport and Dispersion Modeling System: History, Applications, and New Developments. In Proceedings of the Air and Waste Management Association—Guideline on Air Quality Models 2016: The New Path, Chapel Hill, NC, USA, 12–14 April 2016.

40. Rolph, G.; Stein, A.; Stunder, B. Real-Time Environmental Applications and Display SYstem: READY. *Environ. Model. Softw.* **2017**, *95*, 210–228. https://doi.org/10.1016/j.envsoft.2017.06.025.

41. Sahoo, S.; Tiwari, D.K.; Panda, D.; Kundu, B. Eruption Cycles of Mount Etna Triggered by Seasonal Climatic Rainfall. *J. Geodyn.* **2022**, *149*, 101896. https://doi.org/10.1016/j.jog.2021.101896.

42. Alparone, S.C.; Barberi, G.; Di Grazia, G.; Giampiccolo, E.; Maiolino, V.; Mostaccio, A.; Musumeci, C.; Scaltrito, A.; Tuvè, T.; Ursino, A. *Mt. Etna Seismic Catalog 2014–2016*; Istituto Nazionale di Geofisica e Vulcanologia (INGV): Roma, Italy, 2020.

43. Pedley, H.M.; House, M.R.; Waugh, B. The Geology of Malta and Gozo. *Proc. Geol. Assoc.* **1976**, *87*, 325–341. https://doi.org/10.1016/S0016-7878(76)80005-3.

44. Pedley, H.M.; House, M.R.; Waugh, B. The Geology of the Pelagian Block: The Maltese Islands. In *The Ocean. Basins and Margins*; Springer: Boston, MA, USA, 1978.

45. Magri, O. A Geological and Geomorphological Review of the Maltese Islands with Special Reference to the Coastal Zone. *Territoris* **2006**, *6*, 7–26.

46. Cinelli, G.; Tondeur, F.; Dehandschutter, B.; Bossew, P.; Tollefsen, T.; De Cort, M. Mapping Uranium Concentration in Soil: Belgian Experience towards a European Map. *J. Environ. Radioact.* **2017**, *166*, 220–234. https://doi.org/10.1016/j.jenvrad.2016.04.026.

47. Karstens, U.; Schwingshackl, C.; Schmithüsen, D.; Levin, I. A Process-Based 222radon Flux Map for Europe and Its Comparison to Long-Term Observations. *Atmos. Chem. Phys.* **2015**, *15*, 12845–12865. https://doi.org/10.5194/acp-15-12845-2015.

48. Karstens, U.; Levin, I. TraceRadon Monthly Radon Flux Map for Europe 2006–2022 (Based on ERA5-Land Soil Moisture). 2023. Available online: https://hdl.handle.net/11676/XPxf8v5gfDWmi6BZ597euAJ7 (accessed on 2 October 2023).